Studies of Surface Segregation and Surface Properties of *N*-Pentylperfluorooctaneamide End-Capped Semicrystalline Poly(butylene isophthalate) Films

Zhonggang Wang,[†] Dietmar Appelhans,*[,‡] Alla Synytska,[‡] Hartmut Komber,[‡] Frank Simon,[‡] Karina Grundke,*[,‡] and Brigitte Voit[‡]

Department of Polymer Science and Materials, School of Chemical Engineering, Dalian University of Technology, Zhongshan Road 158, Dalian, 116012, People's Republic of China, Leibniz Institute of Polymer Research Dresden, Hohe Straβe 6, D-01069 Dresden, Germany

Received June 4, 2008; Revised Manuscript Received August 29, 2008

ABSTRACT: The surface segregation behavior of a series of *N*-pentyl-perfluorooctaneamide end-capped semicrystalline poly(butylene isophthalate) films (FPBI) was investigated in this work by differential scanning calorimetry, fluorine analysis, contact angle measurements based on axisymmetric drop shape analysis-profile, angle-resolved X-ray photoelectron spectroscopy, ellipsometry and tapping-mode atomic force microscopy (AFM). The fluorine content of the FPBI varied from 0 % to 9.14 wt %. AFM measurements indicated a pin-like topography of the FPBI films. The density of pin-like peaks increased with the increase of the fluorine content, indicating that FPBI chains were well organized in the way that the perfluorinated groups oriented toward the film surface. The high hydrophobicity and oleophobicity together with a high fluorine content in the surface region confirmed that the pin-like peaks were due to aggregates of polymer chains with perfluoroalkyl segments. The F/C atomic ratio at the topmost surface was as high as 0.68 and the CF_3/CF_2 ratio increased significantly from the inner bulk to the film surface.

Introduction

Partially fluorinated polymers have found wide applications as coating materials due to their good chemical/thermal stability, weather-resistance, low friction coefficient, low surface energy, and nonstick behavior.[1−5] From the viewpoint of both cost-saving and good water/oil repellency, it is desirable that most of the fluorinated groups can be segregated to the coating surface. The difference in the surface tension between fluorinated and nonfluorinated moieties of the polymer backbone is the main driving force for the enrichment of fluorinated groups at the coating surface. The fluorine concentration decreases gradually from the outermost surface to the inner bulk. This effect is also known as self-stratification behavior. In this way, very hydrophobic surfaces can be obtained by only small amount of fluorine content in the polymer. So far, partially fluorinated polymers that appeared in the literature include poly(acrylates/methacrylate)s,[6,7] polyarylethers,[8] polysiloxanes,[9] epoxy resins,[10] polyimides,[11,12] polymaleimides,[13,14] polyesters,[15,16] polyurethanes,[17,18] and their random, block, and graft copolymers.[19,20]

In comparison with the large amount of reports on polymers containing fluorinated side chains, the physicochemical and structural studies of polymers with one end or both ends capped by fluorinated groups are rather limited. As a matter of fact, the end-group fluorination method is more attractive considering the ease of synthesis and the chance to obtain a low surface energy of the coating surface while maintaining the preferred bulk properties such as good solubility, melting processability, and film-forming properties. Hirao et al.[21] reported that, for the same polystyrene backbone and similar fluorine content, the fluorinated groups at the end of the polymer chain resulted in significantly higher fluorine enrichment and surface hydrophobicity than that incorporated inside the chain. Elman et al.[22] investigated the distribution of fluorosilane terminated groups of polystyrene at both the air and substrate interfaces, and found that the fluorinated end-groups were depleted from the substrate interface but preferentially aggregated at the air−solid interface. Affrossman et al.[23] also observed that the polystyene end-capped with perfluorooctyldimethylchlorosilane had a strong surface segregation effect.

However, it should be noted that, even though within the same fluorine segment, the surface tension of trifluoromethyl($-CF_3$) (15 mN/m) is much lower than that of difluoromethylene($-CF_2$) (23 mN/m).[24−26] Therefore, in order to achieve the lowest possible surface energy, the surface-segregated fluorinated groups should be well aligned and oriented to the air−film direction so that the $-CF_3$ groups can be exposed to the film surface. For poly(ethylene oxide) end-capped with perfluorodecanoyl groups, through polarized infrared reflectance spectroscopy, Su et al.[27] observed that perfluoroalkyl groups were nearly perpendicular to the air interface, exhibiting excellent surface activity.

A review of the literature reveals that apart from the difference in surface tension between the fluorinated group and other components, a variety of other factors can also affect the segregation ability of fluorinated groups, such as the chemical structure of the polymer main chain, stereoconfiguration, conformation, rigidity, intra- and interchain interaction, molecular weight, degree of crystallinity, glass transition temperature, melting temperature, length of fluorinated segment, film forming process, and thermal history, and so forth. However, until now, the understanding of structure−property relationships is still insufficient. In order to develop polymer coatings with well-organized fluorinated groups on the surface, more fundamental knowledge of the influence of polymer structural parameter on self-stratification behavior of fluorinated groups is essential for both the industrial and academic fields.

Poly(butylene isophthalate) (PBI) is an important thermoplastic resin owing to its excellent melt processability, good mechanical properties and good solubility in common solvents. Similar to other commercial linear polyesters, such as poly(ethylene terephthalate) (PET) and poly(butylenes terephtha-

* To whom all correspondences should be addressed. E-mail: applhans@ipfdd.de and grundke@ipfdd.de.
[†] Dalian University of Technology.
[‡] Leibniz Institute of Polymer Research Dresden.

10.1021/ma8012465 CCC: $40.75
Published on Web 10/22/2008

Scheme 1. Chemical Structure of PBI and FPBI[a]

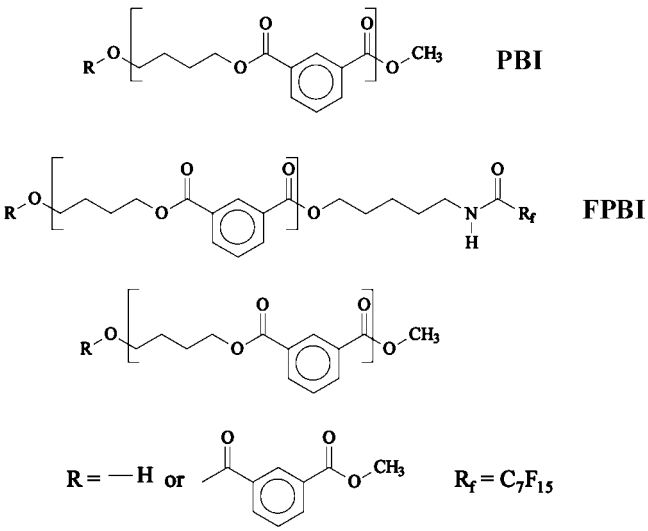

[a] FPBI consists of two polymer backbones at which the non-fluorinated part is reduced by the increasing amount of incorporated R_f-monomer in FPBI.

late)(PBT), PBI is also a semicrystalline polymer, but its degree of crystallinity rate is relatively low.[28,29] The above physicochemical features attracted us to perform some modifications to endow PBI with some new functions.

In the present study, *N*-pentyl-perfluorooctaneamide end-capped semicrystalline poly(butylene isophthalate)s (FPBI) was synthesized in our laboratory. The crystalline characteristic indicates good alignment ability of the polymer chain. The slow crystallization rate provides sufficient time for adjusting the conformation of the polymer chain so that fluorinated groups can migrate to the coating surface. Moreover, the fluorinated group was designed to connect with $(-CH_2-)_5$ spacer via an amide group, which can yield strong intermolecular hydrogen-bonds between fluorinated groups, and thus will be advantageous for the good self-organization and orientation stability of fluorinated groups at the film surface. Their wettability, surface fluorine enrichment, and morphology were investigated by ADSA-P, angle-resolved XPS, and tapping-mode AFM.

Experimental Section

Materials. Butanediol and dimethyl isophthalate were purchased from Aldrich Company, and used as received. The polymerization was carried out using a melting polycondensation method at 200 °C under vacuum, using $Ti(OBu)_4$ as catalyst. The molar ratio ester/OH, including molecular weights of monomers, and the amount of R_f-OH (*N*-(5-hydroxypentyl)perfluorooctaneamide) used for the synthesis and characteristics (M_n, M_w, M_w/M_n, T_g, T_m, and bulk content of fluorine for polyesters) of polyesters are described in Table 1. Structure analysis of polyesters by ^{1}H NMR reveals literature known ^{1}H NMR spectra. Only ^{19}F NMR (Supporting Information) outlines deeper information about the stability of the amide group in adjacent to the perfluoroalkyl segment (C_7F_{15}) after the polycondensation reaction. There is no obvious cleavage of the amide bond during the polycondensation reaction. This means that the potential cleavage product perfluorooctanoic acid in the polycondensation product of the fluorinated polyester is not present. For comparison, the ^{19}F NMR spectrum of the polycondensation reaction of perfluorooctanoic acid, 1,4-butanediol and adipic acid is presented too, which shows the presence of unconverted perfluorooctanoic acid as educt (Supporting Information). The monomer R_f-OH ($M_w = 499.21$ g/mol) was received by following synthetic procedure: 5-Aminopentanol (1.23 g; 11.9 mmol) was dissolved in anhydrous methanol (30 mL) under N_2-atmosphere. Methyl perfluorooctanoate (5.36 g; 12.5 mmol) was slowly added to the reaction solution at room temperature. Then, the reaction mixture was kept at 35 °C overnight followed by the evaporation of the solvent and excess methyl ester. The crude product was dried under high vacuum and was received as pure product with a yield of 91%. Melting point: 62.2−65.9 °C. ^{1}H (DMSO): $\delta = 1.27$ (m, 2H, $CH_2-CH_2-CH_2-OH$); 1.41 (m, 2H, CH_2-CH_2-OH); 1.48 (m, 2H, $CO-NH-CH_2-CH_2$); 3.19 (q, 2H, $CO-NH-CH_2$); 3.36 (m, 2H, CH_2-OH); 3.5 (s, 1H, OH); 9.44 ppm (t, 1H, $CO-NH-CH_2$). ^{13}C (DMSO): $\delta = 22.66$ ($CH_2-CH_2-CH_2-OH$); 28.08 ($CO-NH-CH_2-CH_2-(CH_2)_3-OH$); 31.99 ($CH_2-CH_2-OH$); 39.54 ($CO-NH-CH_2$); 60.51 ($CH_2-OH$); 156.45 ppm (CO). ^{19}F NMR (DMSO): $\delta = -126.0, -122.7, -122.1, 121.7$ ($F_3C-(CF_2)_5-CF_2-CONHR$); −118.9 ($F_3C-(CF_2)_5-CF_2-CO-NHR$); 80.6 ppm ($CF_3$).

The NMR spectroscopic experiments were performed in 5 mm o.d. sample tubes with a Bruker DRX 500 NMR spectrometer at 500.13 MHz for ^{1}H NMR spectra, at 470.59 MHz for ^{19}F NMR spectra and at 125.75 MHz for ^{13}C NMR spectra. DMSO-d_6 was used as solvent for all NMR experiments. For internal calibration, the solvent peaks of DMSO-d_6 were used: δ (^{13}C) = 39.60 ppm; δ (^{1}H) = 2.50 ppm for the analysis of R_f-OH. The ^{19}F NMR spectra were referenced to internal C_6F_6 (δ (^{19}F) = −163 ppm). The signal assignment was done by 2D NMR experiments using the standard pulse sequences provided by Bruker.

Silicon wafers (2 × 2 cm^2) with a round hole of 1 mm in diameter were used as substrates. Before using, wafers were treated with a piranha solution (4: 1 mixture of H_2SO_4 and H_2O_2) at 80 °C for 1 h, then the wafers were rinsed with Millipore water for 30 min, and blew dried with nitrogen stream.

Film Preparations. Silicon wafers on which the films were coated had a native SiO_2 layer of approximately 2 nm. Polymer solutions of 2% concentration in chloroform were filtrated through a 0.25-μm poly(tetrafluoroethylene) filter to remove particles just prior to spin coating. The spin time was 30 s and spin speed was 2000 r/min. At first, the solvent was allowed to evaporate at room temperature for 24 h, then the films were transferred to a vacuum oven, and further dried at 40 °C and 10 mmHg for additional 24 h.

Advancing and receding water (W) and *n*-hexadecane (HD) contact angles were measured by the sessile drop method using axisymmetric drop shape analysis (ADSA-P) and a conventional drop shape technique (Krüss DSA 10, Hamburg, Germany). In this work, at least five dynamic water contact-angle measurements at velocities of about 0.2 mm/min were performed. Low-rate dynamic contact angles at these velocities are essentially identical with the advancing contact angles obtained by the conventional drop shape technique.[30] The latter technique was used to determine advancing and receding *n*-hexadecane (HD) contact angles for prepared films. At least 5 separate measurements for each of 5 samples were used to calculate a mean contact angle. The standard deviation did not exceed 2−3° for advancing and receding contact angles, respectively. All contact angle measurements were carried out at 24° ± 0.5 °C and relative humidity of 40 ± 3%, which were kept constant.

The thickness of spin-coated films was measured by a Multiscope Optrel (Berlin, Germany) null-ellipsometer.[31] Initially, the thickness of the native SiO_2 layer (usually 1.7 ± 0.2 nm) was calculated at refractive indices $N = 3.858\text{-}i0.018$ for the Si substrate and $n = 1.4598$ for the SiO_2 layer. The thickness of polyester layers was evaluated applying the three-layer model Si/SiO_2/FPBI using the measured value $n = 1.7$ for the refractive index of FPBI films. The thickness of the FPBI layers was measured to be in the order of 100 nm.

Tapping mode AFM measurements at room temperature were carried out using a Nanoscope III (Digital Instruments, Santa Barbara). Commercial silicon cantilever with spring constant of 35 N/m and resonance frequency around 285 kHz was used. Unless stated otherwise, the set point amplitude, which is used in feedback control, was adjusted to 40−70% of the free air amplitude for all images. Data analyses were carried out using specifically designed Digital Instruments software (version 5.12r3 Nanoscope software).

Table 1. Conversion Conditions for the Synthesis of Polyesters and Physical Properties of Polyesters Investigated

sample	R_f-OH[a] (wt %)	ratio ester/OH[b]	M_n (g/mol)	M_w (g/mol)	M_w/M_n	T_g (°C)	T_m (°C)	% F bulk (wt %)	R_f-endgroups[c](%)
PBI	0	0.91	2700	6000	2.2	15	129	0	
FPBI-1	1.5	0.98	6300	16200	2.6	19	132	1.01	11
FPBI-2	5	0.95	7100	14600	2.1	13	130	3.01	37
FPBI-3	10	0.95	6600	14700	2.2	17	130	6.15	71
FPBI-4	15	0.98	4100	8400	2.0	15	129	9.14	65

[a] R_f-OH used for polycondensation reaction. [b] Molar ratio consisting of $\times$ mol Ester/(y mol butanediol + z mol R_f-OH) for polycondensation ($M_{w,Ester}$ = 194.19 g/mol, $M_{w,Diol}$ = 90.12 g/mol and $M_{w,Rf\text{-}OH}$ = 499.21 g/mol) at which $\times < (y + z)$ with $y > z$. [c] Details for calculation are presented in the Supporting Information.

The values of root-mean-square roughness (rms) were calculated over the whole captured film area.

Glass transition temperatures (T_g) and melting points (T_m) were determined on a Perkin-Elmer DSC-7, over a temperature interval of −50−170 °C at a heating rate of 10 °C/min. T_g's were read at the middle of the change in the heat capacity from the second heating runs.

Angle-resolved XPS measurements[32] were performed in both survey and high-resolution mode on an Axis Ultra (Kratos Analytical, Manchester, England), with a monochromatized Al Kα ($h\bullet\nu$ = 1486.6 eV) X-ray light source of 300 W at 15 kV. The kinetic energy of the photoelectrons was determined with an hemispheric analyzer set to a pass energy of 160 eV for wide scan spectra and 20 eV for high-resolution spectra, respectively. The spectral background was subtracted according to the Shirley method.[33] The polymer films were mounted on a sample holder and introduced in a separate preparation chamber which was directly connected with the spectrometer. The chamber was quickly evacuated to a base pressure not higher than 2×10^{-8} Torr, then the samples were transferred to the analysis chamber of the spectrometer where the spectra were recorded. During all measurements, electrostatic charging of the sample was avoided by means of a low-energy electron source working in combination with a magnetic immersion lens. All of the recorded peaks were shifted by the same value, which was necessary to set the C_{1s} peak to 285.00 eV.[33]

Fluorine analyses and elemental analyses were carried out by Mikroanalytisches Labor Beller (Göttingen/Germany).

Number- and weight-average molecular weight (M_n and M_w, respectively) of the polymers were determined by a Gel permeation chromatography (GPC) system. Tetrahydrofuran (THF) was used as solvent and eluent with polystyrene standards as reference.

Results and Discussion

N-Pentyl-perfluorooctaneamide end-capped poly(butylene isophthalate)s were synthesized in our laboratory by conventional melting polymerization method from *N*-(5-hydroxypentyl)-perfluorooctaneamide, butanediol, and dimethyl isophthalate. The bulk fluorine contents of fluorinated PBIs (FPBI-1−FPBI-4) were 1.01 wt %, 3.01 wt %, 6.15 wt %, and 9.14 wt %, respectively (Table 1). Slightly excess OH-containing monomers were used toward the diester monomer during the polycondensation reaction (Table 1). Their bulk physical properties, characterized by fluorine elemental analysis, DSC and GPC are listed in Table 1. In fact, the fluorinated polymer thus obtained was a mixture, containing both the unmodified polymer chain of PBI and fluorinated polymer chain of PBI. The higher fluorine in the fluorinated polyester, the higher the content of *N*-pentyl-perfluorooctaneamide end-capped polymer chains of PBI. GPC data showed that all of the polymers synthesized had a broad molecular weight distribution with polydispersity values about 2 (Table 1). Here, it can be seen also that the FPBI-1−FPBI-3 with increasing bulk fluorine content possess similar molecular weights at which the M_w data for FPBI-1 is slightly higher than those of FPBI-2 and FPBI-3. Only FPBI-4 really shows lower GPC data for the molecular weights due to the influence of the largest amounts of R_f-OH as end-capping agent during the polycondensation for FPBI-4.

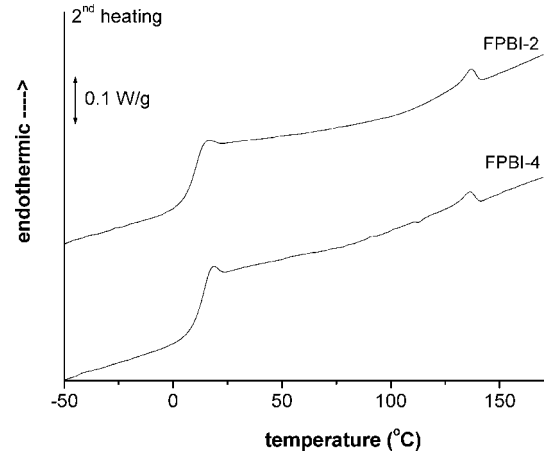

Figure 1. The DSC thermograms of FPBI-2 and FPBI-4.

DSC thermograms for FPBI-2 and FPBI-4 are in Figure 1. DSC results showed that all of the samples had similar glass transitions temperatures (T_g) and melting temperatures (T_m) in the range of 13−19 °C and 129−132 °C, respectively, indicating that the increasing fluorine content did not cause an obvious change in the mobility of the polymer segments. The appearance of crystallization/melting peaks showed that this series of polymers could crystallize to some extent, and this fact again did not depend on the fluorinated end groups. In addition, the samples had good solubility in the common organic solvents, and films could easily be prepared by spin-coating from 2 wt % chloroform solution. The average film thickness was about 100 nm.

Wettability and Film Surface Free Energy. Figures 2 and Figure S of the Supporting Information show typical contact angle patterns for sessile water droplets obtained by ADSA-P measurements on films of FPBI-3 and FPBI-4, respectively. To measure advancing and receding contact angles, the drop volume V is increased and decreased linearly. While the contact radius r of the sessile drop also increases monotonically with a rate of about 0.16 mm/min, the contact angle θ remains very constant as the drop advances. For both films, the advancing contact angles were very high, at a value of 111.5° ± 0.74 (FPBI-3) and 112.2° ± 0.53 (FPBI-4). As pumping of the liquid is reversed after about 450 s, the drop volume starts to decrease linearly, and the contact angle decreases at constant drop contact radius r. At a certain point, the three-phase line starts to move again while the contact angle is roughly constant resulting in a receding contact angle θ_r. For the FPBI-3 film, θ_r is 85.7°. In the case of the FPBI-4 film, θ_r was determined to be 90.7°.

The variations of the water advancing and receding contact angles as a function of the bulk fluorine content in FPBIs are illustrated in Figure 3. From the nonfluorinated PBI film to the FPBI-2 film, a relatively strong increase of the measured advancing contact angle of water was observed starting from 78° for the nonfluorinated film to 103.5° for the FPBI-2 film. This increase is caused by a bulk fluorine of only 3.01 wt % for FPBI-2. Thus, a very hydrophobic film surface was

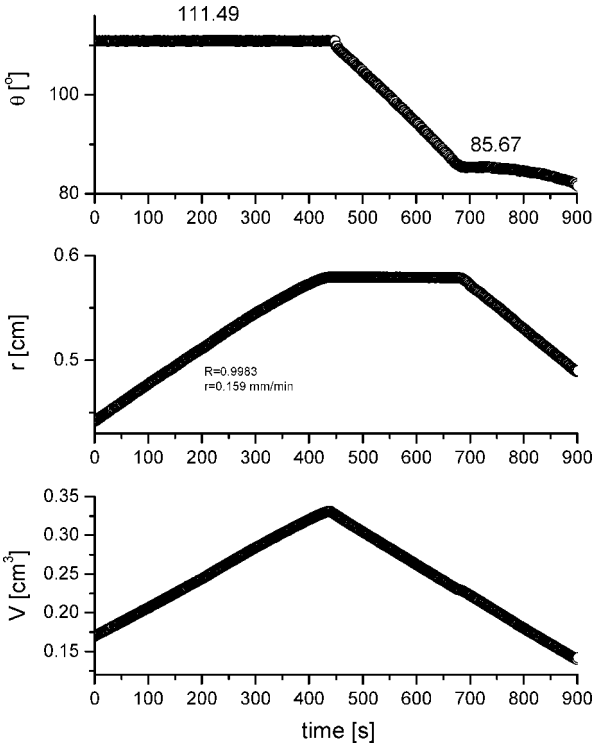

Figure 2. ADSA-P graph of FPBI-3 film.

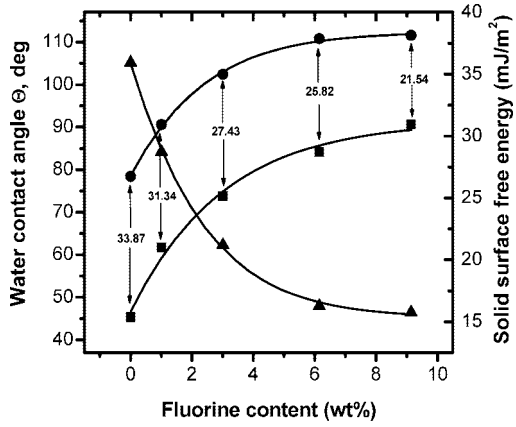

Figure 3. The relationship plots of contact angle, surface tension, and contact angle hysteresis versus fluorine content for the five polymer films: (•) Adv. contact angle; (■) Rec. contact angle; and (▲) solid surface free energy.

exhibited. Then, the water advancing contact angle increases further until the bulk fluorine content reached the value of 6.15 wt %. When the bulk fluorine content was further increased to the value of 9.14 wt %, the advancing contact angle did not reflect these changes in the bulk composition. Interestingly, similar contact angles were obtained for the system with about 6 wt % of fluorine, as compared to previous studies in which partially fluorinated oligoesters were used with similar fluorine content.[34] Generally, the contact angle of a drop of a liquid advancing on a solid surface (θ_a) is different from that obtained when it is receding (θ_r). The difference is known as contact angle hysteresis (θ_{hyst}). This phenomenon is often attributed to surface roughness and surface heterogeneity. However, there are several other causes for contact angle hysteresis: molecular scale topography and rigidity of molecules, change in the organization of molecules of the solid surface, penetration of liquid and swelling of the solid, liquid retention, and strong interactions between molecules of solid and liquid.[35]

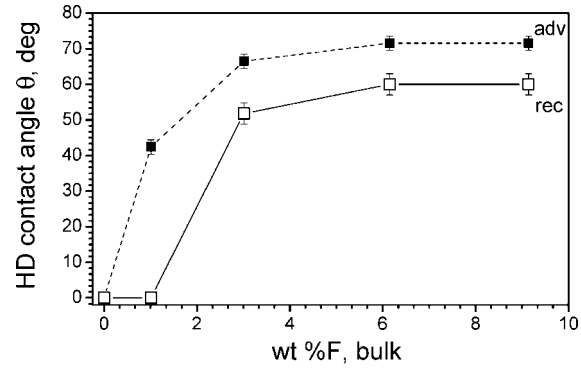

Figure 4. Mean *n*-hexadecane advancing (θ_A^{HD}, solid symbols) and receding (θ_R^{HD}, open symbols) contact angles for investigated polyesters.

Table 2. F/C Enrichment Data from the Angle-Resolved XPS Spectra

sample	F-content (wt %)	information depth (nm)	bulk F/C atomic ratio	surface F/C atomic ratio[a]	fluorine enrichment factor[b] (Q)
FPBI-1	1.01	2	0.0102	0.0474	4.6
		4		0.0455	4.5
		8		0.0454	4.5
FPBI-2	3.01	2	0.0275	0.363	13.2
		4		0.351	12.8
		8		0.196	7.1
FPBI-3	6.15	2	0.0559	0.533	9.5
		4		0.484	8.7
		8		0.364	6.5
FPBI-4	9.14	2	0.0803	0.683	8.5
		4		0.618	7.7
		8		0.510	6.4

[a] Obtained from F_{1s} and C_{1s} peak area of ARXPS spectra at 2, 4, and 8 nm information depths. [b] *Q* is the ratio of surface F/C atomic ratio to bulk F/C atomic ratio.

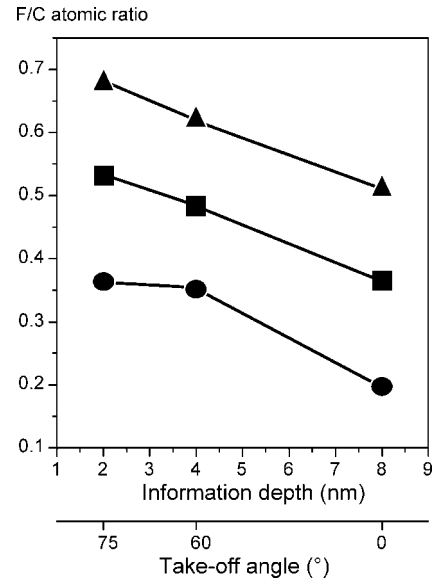

Figure 5. F/C atomic ratio versus information depth of the three polymer films: (▲) FPBI-4; (□)FPBI-3; and (●) FPBI-2.

For the study and evaluation of surface hydrophobicity, the values of advancing and receding contact angles should be considered.[5,7,34,36] As can be seen from Figure 3, for our samples, the receding water contact angles show a similar trend with increasing bulk fluorine content compared to those of the advancing contact angles. Moreover, it is remarkable that the nonfluorinated PBI (fluorine content 0 wt %) possessed the

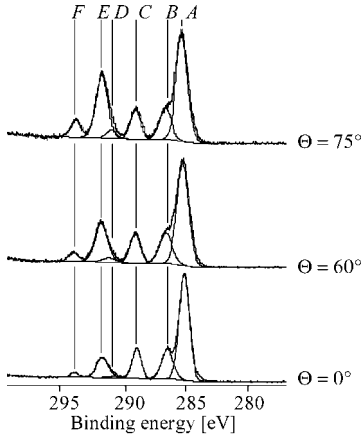

Figure 6. High-resolved C_{1s} spectra at different take-off angles for FPBI-4 film.

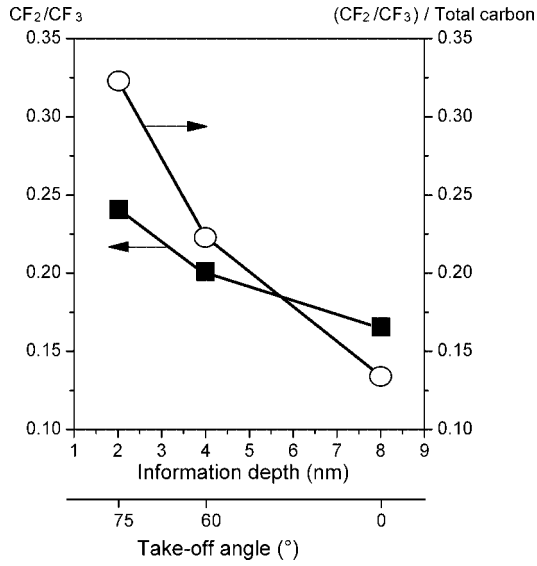

Figure 7. Plots of ratios of CF_3/CF_2 and $(CF_3 + CF_2)$/(total carbon) versus information depth for FPBI-4 film.

largest water contact angle hysteresis of 33.87°and the hysteresis values decreased with the increase of the fluorine content (Figure 3). With the incorporation of increasing amounts of fluorinated groups, the interaction of the water with the polar groups on the surface will be more strongly prevented. This causes a higher receding contact angle. The reasons responsible for the lowering of the contact angle hysteresis are unknown considering only the contact angle measurements. Further details are revealed by XPS and AFM measurements, presented and discussed below.

Further measurements were done to receive additional information about the oleophobicity of the fluorinated PBI films. Figure 4 summarizes the hexadecane (HD) advancing (θ_A^{HD}) and receding (θ_R^{HD}) contact angles on the polyester surfaces as a function of the bulk fluorine content. In the case of the nonfluorinated PBI film, *n*-hexadecane wets the surface completely.

A further increase in the bulk fluorine content leads to a simultaneous increase in advancing and receding HD contact angles. For the lowest fluorine content ($F = 1.01$ wt %), an advancing HD contact angle of 42.4° was measured (Figure 4). Apparently, incorporation of a negligible amount of fluorinated species (about 1 wt %) into the polyester results in a strong increase of *n*-hexadecane advancing contact angle. However, the HD receding contact angle remains zero. The addition of more fluorine in the system (about 3 wt %) results in further increase in both the *n*-hexadecane advancing and receding contact angles (Figure 4). Similar to water, the HD advancing contact angle steadily increased (up to 72°) until the bulk fluorine content reached the value of 6.15 wt % and then remained constant at higher fluorine concentration (9.14 wt %) (Figure 4). These results are also in reasonable agreement with previously reported ones for perfluorinated oligoesters.[34] In this case, the HD advancing contact angles reached plateau values (about 80°) at higher fluorine concentrations (6.24 and 10.72 wt %). Ming et al. have reported similar wetting behavior of *n*-hexadecane on partially fluorinated non- and blocked (poly)-isocyanates.[16,41]

It should be noted that the HD contact angle hysteresis is rather small for the samples with the highest fluorine content (6.15 and 9.14 wt %) and is of about 12°. Thereby, fluorinated polyesters with higher fluorine contents possess oleophobic surface properties. Obviously, the investigated perfluoroalkyl segment adjacent to the amide group is an equivalent moiety in comparison to other perfluoroalkyl moieties, described in literature, in order to create films with very hydrophobic and oleophobic surface properties.

The advancing water and hexadecane contact angles were used to calculate the solid surface free energy γ_{sv} using the equation of state approach (EQS) for solid−liquid interfacial tensions:[37,38]

$$1 + \cos\theta = 2\sqrt{\frac{\gamma_{sv}}{\gamma_{lv}}}e^{-\beta(\gamma_{lv} - \gamma_{sv})^2} \quad (1)$$

where β is an empirical parameter and was found to be 0.0001247 $(mN/m)^{-2}$, γ_{sv},γ_{lv} denote the interfacial free energies of the solid−vapor and liquid−vapor interfaces, respectively; θ is the liquid contact angle. The assumptions behind eq 1 are based on the strategy to measure the contact angles of well-defined model liquids on a solid surface and to relate the results to the surface energetics using Young's equation. It should be noted that many questions still remain regarding the validity and applicability of Young's equation. Young's equation predicts a single value for the contact angle because the equilibrium contact angle in Young's equation, θ_Y, is a unique function of the interfacial tensions γ_{sv}, γ_{sl}, and γ_{lv}. But on real solid surfaces, contact angle phenomena can be very complicated and contact angle hysteresis between advancing and receding contact angles is observed (see results of this work). Therefore, the thermodynamic status of contact angles is often unclear and experimentally observed apparent contact angles, θ_{ap}, may or may not be equal to the Young contact angle θ_Y. It was concluded that the experimental advancing contact angle, θ_a, on a smooth, but chemically heterogeneous solid surface can be expected to be a good approximation of θ_Y. While the receding angle on a heterogeneous and smooth surface can also be a Young contact angle, it is often found to be unreproducible and time-dependent.

The solid surface free energy values calculated from the advancing contact angle of water for the five polymer films are shown in Figure 3. The solid surface free energy of the nonfluorinated PBI film was calculated to be 35.8 mJ/m^2, which is well consistent with the literature values of the critical surface tension for other nonfluorinated polyester materials.[20,34,39,40] With the increase of fluorine content, the film surface free energies decreased from 35.8 mJ/m^2 for PBI down to 15.7 mJ/m^2 for FPBI-4, which is even lower than that of poly(tetrafluoroethylene) (18.5 mJ/m^2).[24]

However, there is some inconsistency between the values of the surface free energy calculated from the experimental values of water and *n*-hexadecane advancing contact angles for the nonfluorinated (PBI) and films with lower bulk fluorine contents

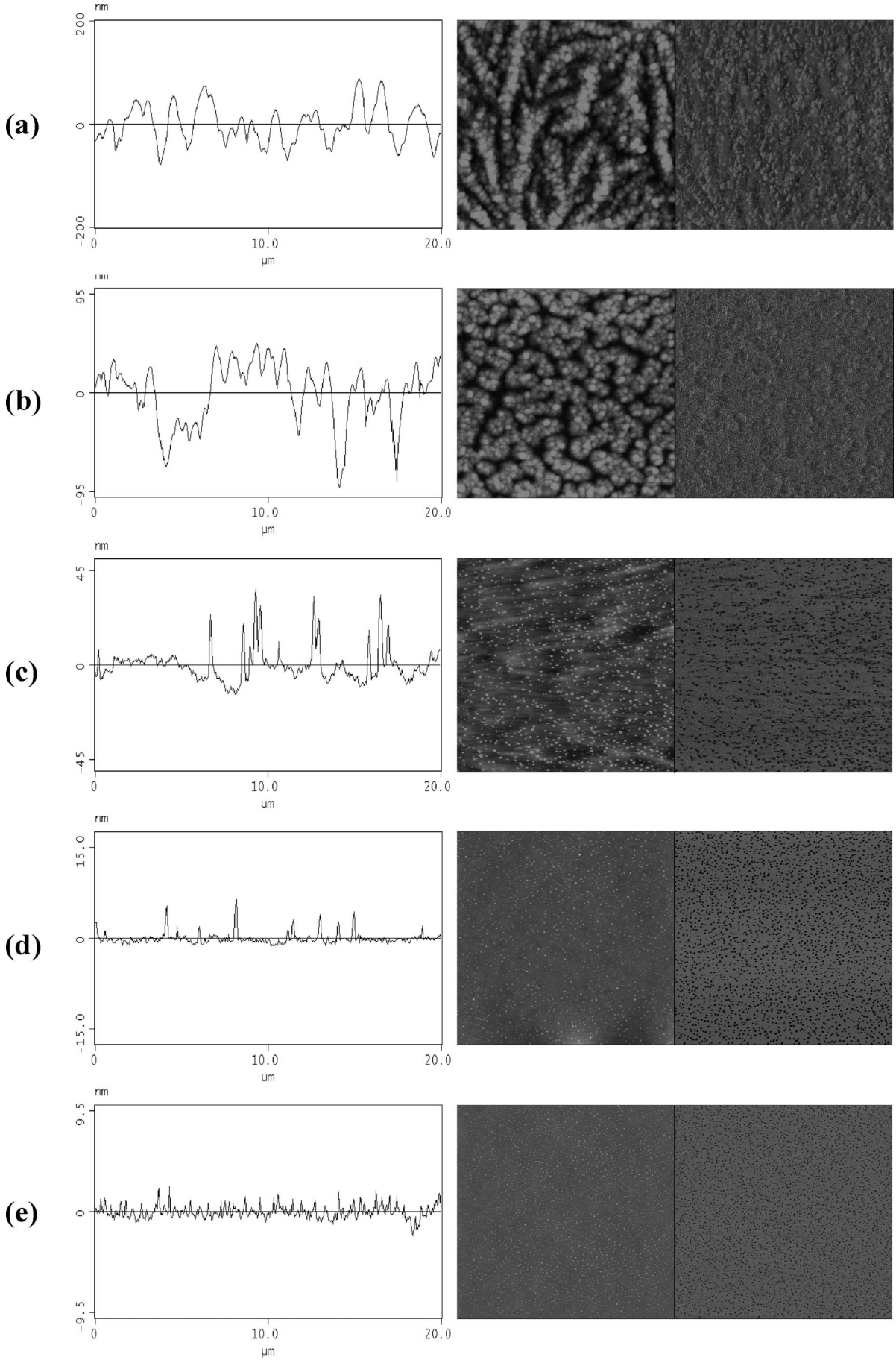

Figure 8. AFM height (left), phase (right) images and section profiles of the five polymer films: (a) PBI, (b) FPBI-1, (c) FPBI-2, (d) FPBI-3, and (e) FPBI-4.

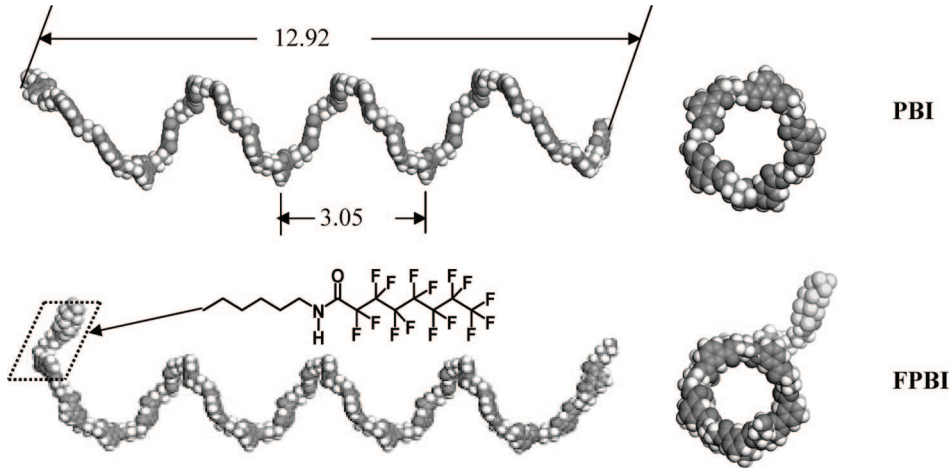

Figure 9. Chain conformations of PBI and FPBI containing 20 repeating units. (left) side view; (right) view in the direction of main chain.

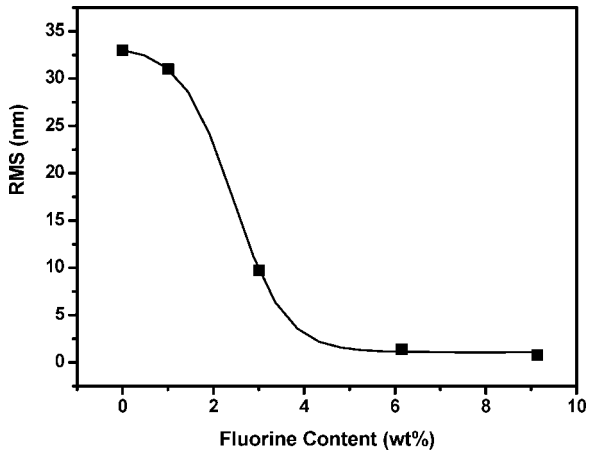

Figure 10. Variation of roughness (rms) values with fluorine content for the five polymer films.

in the range from % $F = 1.01$ wt % to % $F = 3.01$ wt %. The calculated solid surface free energy from the HD contact angle values ranges from $\gamma_{sv} = 27.5$ mJ/m^2 (% $F = 0.00$ wt %) to $\gamma_{sv} = 21.0$ mJ/m^2 (% $F = 1.01$ wt %) and $\gamma_{sv} = 14.1$ mJ/m^2 (% $F = 3.01$ wt %), whereas the values based on water contact angles between 35.8 mJ/m^2 for PBI down to $\gamma_{sv} = 28.7$ mJ/m^2 (% $F = 1.01$ wt %) and $\gamma_{sv} = 21.2$ mJ/m^2 for the % $F = 3.01$ wt % bulk fluorine contents, respectively. Note, surface free energy values obtained from advancing water contact angle are consistent with those obtained using HD contact angles for highly fluorinated samples FPBI-3 and FPBI-4 (% $F = 6.15$ and 9.14 wt %, respectively). One reason might be that systems with 0, 1.01, and 3.01 wt % fluorine contents are not homogeneous and possess some level of surface roughness (Figure 10). Increasing the fluorine concentration in the system, however, leads to a rise in the chemical heterogeneities on the one hand and smoothening/leveling effects on the other (Figure 10). This supports the idea that the experimental advancing contact angle, θ_a, on a smooth, but chemically heterogeneous solid surface can be expected to be a good approximation of θ_Y and results in consistent values of surface free energy calculated from W and HD contact angles by use of EQS.

XPS Depth Profiling of Fluorinated PBI Films. Angle-resolved XPS is a useful tool for investigation of fluorine enrichment at the outermost film surface due to its good surface sensitivity and capability of providing chemical bonding information. For polymers, the surface sensitivity of the XPS method can be enhanced by tilting the takeoff angle θ, where it is defined as the angle between the sample surface normal and the optical axis of the photoelectron spectrometer. XPS spectra were performed at three takeoff angles: 0°, 60°, and 75°, corresponding to the information depths of ~8, 4, and 2 nm, respectively.

The fluorine over carbon (F/C) atomic ratios measured from XPS at different incidence angles are given in Table 2, and the theoretical F/C values in the bulk calculated according to the elemental analysis results are also listed as a comparison. Compared to the low F/C ratio in the bulk, the fluorine species at the surface had a generally pronounced enrichment for the surface F/C atomic ratio to the topmost surface of the fluorinated PBI films (Table 2).

Figure 5 shows a plot of F/C atomic ratios versus information depth for three polymer films. A gradient in the fluorine concentration from the outermost surface down to an information depth of about 8 nm was detected. The fluorine concentration was distinctly higher at the topmost film surface. For sample FPBI-4, which has a bulk fluorine content of 9.14 wt %, the F/C atomic ratio even reaches 0.68 at the surface of 2 nm depth. In addition, since the fluorinated moiety was connected with the polyester chain via an amide group, the variations of N/C atomic ratio with information depth should also exhibit a similar trend as the F/C ratios. Figure S (Supporting Information) confirms this behavior. This indicates also that the self-stratification properties of the *N*-pentyl-perfluorooctaneamide end group in the outermost surface are well suited to create films with very hydrophobic and oleophobic surface properties.

As a measure of the enrichment extent of fluorine on the film surface, a term named enrichment factor (Q; Table 2) is introduced in this study, which is defined as the ratio of the surface fluorine concentration to the bulk one. For FPBI-1 (F-content 1.01 wt %), the film surface exhibited obviously an increase of fluorine concentration, with the Q value of 4.6 (Table 2). The surface enrichment by fluorine was much more significant for the sample FPBI-2, which allowed a fluorine excess at the surface of 13.2-fold more than that of the bulk level. A further increase of fluorine in the bulk led to the drop in the enrichment factor. For FPBI-3 and FPBI-4, the Q values were 9.5 and 8.5, respectively. This phenomenon was also observed for other fluorinated polyester systems. It is assumed that the perfluorinated groups in the topmost surface layer hamper the migration of additional perfluorinated moieties to the surface when the bulk fluorine content reaches a certain level.[34]

To further investigate the orientation state of perfluorinated end-groups at the surface, high-resolution resolved C_{1s} spectra were recorded. The spectra were dissected by means of the spectra deconvolution software. The discrete peaks were as-

signed to different carbon-based functional groups, and their contents could be calculated from the relative peak areas of the individual carbon components. The parameters of component peaks were their binding energy, height, full width at half-maximum, and the Gaussian−Lorentzian ratio.

Typical angle-resolved C_{1s} spectra for the sample of FPBI-4 at different takeoff angles are given in Figure 6. The peak at the binding energy of 284.7 eV (A) was attributed to the carbon atoms of phenyl ring and aliphatic $-CH_2-$ segments. The signal of 286.3 eV (B) was assigned to the carbons bonded to oxygen or nitrogen atoms. The peak at 288.6 eV (C) showed the presence of carbonyl carbon of ester groups, whereas the peak at 290.9 eV (D) was assigned to the carbonyl carbon of *N*-pentyl-perfluorooctaneamide group. The signals of CF_3 and CF_2 groups were found to be at 293.9 eV (F) and 291.7 eV (E), respectively. As shown in Figure 7, the relative area ratio of (CF_3 + CF_2) to the total carbon apparently increased with the decrease of information depths. Moreover, for the perfluorinated end-group, the theoretical ratio of CF_3/CF_2 is 1/7 (0.166) which reflects the case that the film surface is saturated with perfluorinated groups and all of them lie flat at the surface. In contrast, the experimental value of CF_3/CF_2 ratio was 0.246, much higher than the theoretical value. This indicates that the fluorinated chains at the surface oriented perpendicularly to the surface and a film with exposed CF_3 group could be formed.

Morphological Investigation on Film Surfaces. The above XPS analysis gave the chemical composition information for 2−8 nm surface depth. To obtain the direct evidence of fluorine aggregation on the topmost surface of polymer films, AFM height and phase images (20 × 20 μm^2) were simultaneously recorded. For AFM measurements at moderate force tapping mode, the height images reveal surface topography, whereas the phase images can provide information about variations in surface stiffness. Moreover, one can also conclude under the consideration of the molecular composition of polyesters used in this study that the dark part in the phase image can be assigned to the soft moiety, and the bright part can be attributed to the stiffer moiety.[42] The evolution of phase (right) and height (left) images as well as their topography section profiles of the five polymer films are illustrated in Figure 8.

In this work, all of the thin films of FPBIs and nonfluorinated PBI were prepared by the spin-coating method from their dilute chloroform solutions, with average thickness of about 100 nm. Chloroform is a very easily volatile solvent, so in the course of film-forming, there is not enough time for PBI chains to arrange their conformations to obtain an ordered chain packing. For the PBI film, the ribbon-like topography was attributed to the disordered polycrystalline aggregates, being situated flat on the surface. The aggregates were typically 8−9 nm high and 1−2 μm wide. In the phase image, the crystalline ribbons appeared brighter than the amorphous surrounding due to their greater stiffness. Similar phenomena have also been observed by the AFM method for other polymer systems, such as poly(diethylsiloxane),[42] ultrathin film of poly(ethylene oxide)/poly(methyl methacrylate) blend,[43] fluorochemical-doped polypropylene,[44] and polyurethane,[45] and so forth. After the end groups were capped with fluorinated group, for FPBI-1, which has only 1.01 wt % of fluorine content, the polycrystalline ribbon aggregates became curled up and transformed into worm-like patterns. In order to explain this interesting phenomenon, molecular modeling was carried out for both PBI and FPBI. As illustrated in Figure 9, the energy-minimized chain of PBI takes a helical conformation with a helical pitch of 3.05 nm. The FPBI main chain has a similar conformation to that of PBI. However, the fluorinated group does not follow the helical direction of PBI or is wrapped within the screw, but obviously stretches out of the helix (Figure 9).

As mentioned above, the samples FPBI-1, FPBI-2, FPBI-3, and FPBI-4 are mixtures of fluorinated polymer chains and nonfluorinated polymer chain, in which only part of the PBI chains with perfluoroalkyl end groups is important for the tailoring of the hydrophobicitiy of surfaces for the FPBI films. Together with the XPS and wettability results, it is assumed to be due to the great difference between the fluorinated group and the polyester backbone, that the perfluoroalkyl head drags the polymer chain to migrate onto the film−air interface. Therefore, the fluorinated moiety points upward with exposed CF_3 group at the topmost layer, leaving the polyester backbone in the inner layer. For the nonfluorinated PBIs, most of them remain in the bulk, close to the substrate. Therefore, the film surface topography reflected the packing characteristics of fluorinated polymer chains to a large extent.

With increasing amounts of fluorinated chains in the samples, the tendency of enrichment of fluorinated chain at the film surface became more and more apparent in the AFM results. For FPBI-2 (Figure 8c), which has fluorine enrichment at the surface 13-fold higher than that in the bulk, only a trace of the crystalline feature of PBI could be detected from its topography image. Alternatively, some pin-like peaks appeared at the surface, which are displayed as dark points in the phase images too. These pin-like peaks have lateral dimensions up to several 100 nm and heights up to 30 nm. The appearance of pin-like peaks changes and becomes denser for FPBI-3 and FPBI-4 with the highest fluorine content in the bulk phase (Figure 8, parts d and e). They become smaller for the lateral dimension and also, the height of the pin-like peaks is with $\leq$3 nm, as presented in the height images of FPBI-3 and FPBI-4, lower. Therefore, a smoothening of the FPBI surface is given (Figure 10). The film surfaces of PBI (Figure 9a) were very rough with rms roughness values of 33 nm (Figure 10). Then the rms values decreased rapidly to 9.7, 1.1, and 0.83 nm, for FPBI-2, FPBI-3, and FPBI-4, respectively (Figure 10). It is believed that the rough surfaces of PBI and FPBI-1 layers were caused by the crystalline characteristics of PBI chains. With the increase of fluorine content, a layer of the fluorinated component, the thickness of which depended on the fluorine content, gradually covered the film surface. Furthermore, the phase images (Figure 8c−e; enlarged phase images in Supporting Information) exhibit the presence of hard and soft phases. The soft phases, presented as dark spots in Figure 8c−e, were attributed to the preferably self-aggregated perfluoroalkyl segments of FPBI on the topmost surface. The self-aggregation of perfluoroalkyl segments on the topmost surface is also supported by strong intermolecular hydrogen bonds between amide bonds in FPBI. In most cases, the position of the soft phase as dark spots in phase images correlates very well with the appearance of the pin-like peaks in the height images. Finally, the results by AFM study support the aforementioned hydro-/oleophobicity results on the fluorinated PBI films, allowing the conclusion that the reduction of surface roughness contributes as one important fact to minimize the contact angle hysteresis.

Conclusions

In this work, the wettability, surface chemical composition, and morphology of *N*-pentyl-perfluorooctaneamide end-capped semicrystalline poly(butylene isophthalate) (PBI) films with different fluorine contents were studied. It was found that the surface free energies decreased from 35.8 mJ/m^2 to a plateau value of 15.7 mJ/m^2 for nonfluorinated PBI and fluorinated FPBI-4 with a fluorine content of 9.14 wt %, respectively. This value is found to be even lower than that of poly(tetrafluoroethylene). Moreover, fluorinated polyesters with fluorine contents of 6.14 and 9.14 wt % possess oleophobic properties. The evolution of surface free energies were compared and discussed

in correlation with angle-resolved XPS analysis results. It was shown that there was an obvious gradient distribution of the fluorine concentration from the surface down to the inner bulk. The experimental value of the ratio of CF_3/CF_2 was found to be 0.246 for FPBI-4 at a 2 nm information depth that is higher than the theoretical one calculated for perfluoralkyl groups lying flat on the surface. Furthermore, it was clearly observed by AFM that after end-capping with perfluorinated groups, a pin-like topography appeared for the polymer films, and the pin density increased with increasing fluorine content, demonstrating that the fluorinated PBI films possessed not only a significantly enriched fluorine surface but also that the perfluoroalkyl groups were well oriented to the surface with the CF_3 groups pointed toward the air−film interface. Finally, the perfluorooctaneamide end group used in this study is an equivalent perfluoroalkyl segment for the establishment of very hydrophobic/oleophobic surfaces obtained from semicristalline polyester films. Furthermore, the perfluorooctaneamide derivative is suited to use for polycondensation reactions under melting conditions. This opens a potential use for the synthetic application under industrial conditions to produce fluorinated polyesters.

Supporting Information Available: The following additional data and spectra are presented: ^{19}F-NMR spectra of fluorinated FPBI-4 compared with fluorinated polyester possessing free perfluorooctanoic acid; ADSA-p graph for FPBI-4, N/C atomic ratio versus information depth for FPBI-2 - FPBI-4 and enlarged AFM height and phase images for PBI and FPBI-1 - FPBI-4. This material is available free of charge via the Internet at http://pubs.acs.org.

Acknowledgment. This work was financially supported by the German Ministry of Education and Research (BMBF) (Project No 01 RC 0040). We are grateful to Mr. Dieter Pleul for XPS measurements, Mrs. Häuβler for DSC measurements and Mrs. Treppe for GPC measurements.

References and Notes

(1) Bertani, R.; Metrangolo, P.; Moiana, A.; Perez, E.; Pilati, T.; Resnati, G.; Rico-Lattes, I.; Sassi, A. *Adv. Mater.* **2002**, *14*, 1197.
(2) Diaz, A. M.; Zolotukhin, M. G.; Fomine, S.; Salcedo, R.; Manero, O.; Cedillo, G.; Velasco, V. M.; Guzman, M. T.; Fritsch, D.; Khalizov, A. F. *Macromol. Rapid Commun.* **2007**, *28*, 183.
(3) Sauguet, L.; Boyer, C.; Ameduri, B.; Boutevin, B. *Macromolecules* **2007**, *39*, 9087.
(4) Krishnan, S.; Ward, R. J.; Hexemer, A.; Sohn, K. E.; Lee, K. L.; Angert, E. R.; Fischer, D. A.; Kramer, E. J.; Ober, C. K. *Langmuir* **2006**, *22*, 11255.
(5) McCloskey, C. B.; Yip, C. M.; Santerre, J. P. *Macromolecules* **2002**, *35*, 924.
(6) Pittman, A. G.; Wall, L. A. *Fluoropolymers*; Wiley Interscience: New York, 1971.
(7) Schmidt, D. L.; Coburn, C. E.; Dekoven, B. M.; Potter, G. E.; Meyers, G. F.; Fischer, D. A. *Nature* **1994**, *368*, 39.
(8) Liu, B. J.; Robertson, G. P.; Guiver, M. D.; Shi, Z. Q.; Navessin, T.; Holdcroft, S. *Macromol. Rapid Commun.* **2006**, *27*, 1411.
(9) Furukawa, Y.; Kotera, M. *J. Appl. Polym. Sci.* **2003**, *87*, 1085.
(10) Laven, J.; Niemantsverdriet, J. W.; Linde, R. *Polymer* **2005**, *46*, 10531.
(11) Yang, C. P.; Su, Y. Y.; Hsiao, S. H. *J. Polym. Sci., Part A: Polym. Chem.* **2006**, *44*, 5909.
(12) Kute, V.; Banerjee, S. *J. Appl. Polym. Sci.* **2007**, *103*, 3025.
(13) Tavana, H.; Appelhans, D.; Zhuang, R. C.; Zschoche, S.; Grundke, K.; Hair, M. L.; Neumann, A. W. *Colloid Polym. Sci.* **2006**, *284*, 497.
(14) Appelhans, D.; Wang, Z. G.; Zschoche, S.; Zhuang, R. C.; Haussler, L.; Friedel, P.; Simon, F.; Jehnichen, D.; Grundke, K.; Eichhorn, K. J.; Komber, H.; Voit, B. *Macromolecules* **2005**, *38*, 1655.
(15) Darras, V.; Fichet, O.; Perrot, F.; Boileau, S.; Teyssie, D. *Polymer* **2007**, *48*, 687.
(16) Ming, W.; Tian, M.; Grampel, R. D.; Melis, F.; Jia, X.; Loos, J.; Linde, R. *Macromolecules* **2002**, *35*, 6920.
(17) Wang, L. F.; Wei, Y. H. *Colloids Surf. B* **2005**, *41*, 249.
(18) Tan, H.; Xie, X. Y.; Li, J. H.; Zhong, Y. P.; Fu, Q. *Polymer* **2004**, *45*, 1495.
(19) Valade, D.; Boyer, C.; Ameduri, B.; Boutevin, B. *Macromolecules* **2006**, *39*, 8639.
(20) Wang, W. C.; Vora, R. H.; Kang, E. T.; Neoh, K. G.; Ong, C. K.; Chen, L. F. *Adv. Mater.* **2004**, *16*, 54.
(21) Hirao, A.; Koide, G.; Sugiyama, K. *Macromolecules* **2002**, *35*, 7642.
(22) Elman, J. F.; Johs, B. D.; Long, T. E.; Koberstein, J. T. *Macromolecules* **1994**, *27*, 5341.
(23) Affrossman, S.; Bertrand, P.; Hartshorne, M.; Kiff, T.; Leonard, D.; Pethrick, R. A.; Richards, R. W. *Macromolecules* **1996**, *29*, 5432.
(24) Wu, S. H. *Polymer Interfaces and Adhesion*; Marcel Dekker: New York, 1982.
(25) Lau, Y. W.; Burns, C. M. *J. Polym. Sci., Part A: Polym. Phys.* **1974**, *12*, 431.
(26) Beernett, M. K.; Zisman, W. A. *J. Phys. Chem.* **1960**, *64*, 1292.
(27) Su, Z. H.; McCarthy, T. J.; Hsu, S. L.; Stidham, H. D.; Fan, Z. Y.; Wu, D. C. *Polymer* **1998**, *39*, 4655.
(28) Pang, K.; Kotek, R.; Tonelli, A. *Prog. Polym. Sci.* **2006**, *31*, 1009.
(29) Sanz, A.; Nogales, A.; Ezquerra, T. A.; Lotti, N.; Munari, A.; Funari, S. S. *Polymer* **2006**, *47*, 1281.
(30) Kwok, D. Y.; Gietzelt, T.; Grundke, K.; Jacobasch, H.-J.; Neumann, A. W. *Langmuir* **1997**, *13*, 2880.
(31) Lloyd, T. B.; Dwight, D. W. Surface Thermodynamics. In *Characterization of Polymers*; Tong, H., Kowalczyk, S. P., Saraf, R., Chou, N. J., Fitzpatrick, L. E., Eds.; Butterworth Heinemann: New York, 1994.
(32) Seah, M. P. In *Practical Surface Analysis by Auger and X-ray Photoelectron Spectroscopy*; Briggs, D., Seah, M. P., Eds.; Wiley: Chincester, 1990; pp 202−255.
(33) Shirley, D. A. *Phys. Rev.* **1972**, *B5*, 58.
(34) Synytska, A.; Appelhans, D.; Wang, Z. G.; Simon, F.; Lehmann, F.; Stamm, M.; Grundke, K. *Macromolecules* **2007**, *40*, 297.
(35) Tavana, H.; Jehnichen, D.; Grundke, K.; Hair, M. L.; Neumann, A. W. *Adv. Colloid Interface Sci.* **2007**, *236*, 134–135.
(36) Spelt, J. K.; Li, D. The Equation of State Approach to Interfacial Tensions. In *Applied Surface Thermodynamics*; Neumann, A. W., Spelt, J. K., Eds.; *Surfactant Science Series*; Marcel Dekker, New York, 1996, Vol. *63*, pp 239−292.
(37) Kwok, D. Y.; Neumann, A. W. *Adv. Colloid Interface Sci.* **1999**, *81*, 167.
(38) Grundke, K. In *Molecular Interfacial Phenomena of Polymers and Biopolymers*; Chen, P., Ed., CRC Press: Boca Raton, 2005; Vol. *10*, pp 323−374.
(39) Sauer, B. B.; McLean, R. S.; Thomas, R. R. *Langmuir* **1998**, *14*, 3045.
(40) Adamson, A. W. In *Physical Chemistry of Surfaces, 5th ed.*; Wiley: New York, 1990; p 368.
(41) van Ravenstein, L.; Ming, W.; van de Grampel, R. D.; van der Linde, R.; de With, G.; Loontjens, T.; Thune, P. C.; Niemantsverdriet, J. W. *Macromolecules* **2004**, *37*, 408.
(42) Magonov, S. N.; Elings, V. *Polymer* **1997**, *38*, 297.
(43) Wang, M. T.; Braun, H. G.; Meyer, E. *Macromolecules* **2004**, *37*, 437.
(44) Ebbens, S. J.; Badyal, J. P. S. *Langmuir* **2001**, *17*, 4050.
(45) Tan, H.; Guo, M.; Du, R. N.; Xie, X. Y.; Li, J. H.; Zhong, Y. P.; Fu, Q. *Polymer* **2004**, *45*, 1647.

MA8012465